

Design issues in ionized metal physical vapor deposition of copper

Michael J. Grapperhaus^{a)}

Department of Nuclear Engineering, University of Illinois, 1406 West Green Street, Urbana, Illinois 61801

Zoran Krivokapic^{b)}

Advanced Micro Devices, MS 117, 915 De Guigne Drive, Sunnyvale, California 94088-3453

Mark J. Kushner^{c)}

Department of Electrical and Computer Engineering, University of Illinois, 1406 West Green Street, Urbana, Illinois 61801

(Received 7 July 1997; accepted for publication 23 September 1997)

The filling of deep vias and trenches with metal for interconnect layers in microelectronic devices requires anisotropic deposition techniques to avoid formation of voids. Ionized metal physical vapor deposition (IMPVD) is a process which is being developed to address this need. In IMPVD, a magnetron sputter deposition source is augmented with a secondary plasma source with the goal of ionizing a large fraction of the metal atoms. Application of a bias to the substrate results in an anisotropic flux of metal ions for deposition. The ion flux also contributes to "sputter back" of metal deposits on the lip of the via which could lead to void formation. In this article, we describe and present results from a two-dimensional plasma model for IMPVD using a dc magnetron and an inductively coupled auxiliary ionization source. The scaling of copper IMPVD is discussed as a function of buffer gas pressure, sputter source, and source geometry. We show that the deposition rate of metal on the substrate will be reduced as pressure increases due to the increase in diffusive losses. We also show that the sputtering of the auxiliary coils can be a significant issue in IMPVD systems, which must be addressed in tool design. © 1998 American Institute of Physics. [S0021-8979(98)02701-7]

I. INTRODUCTION

As microelectronic device dimensions continue to shrink, the filling of vias between metalization layers during fabrication of microelectronic devices increasingly requires anisotropic deposition fluxes to prevent void formation. One technique that shows great promise in this regard is ionized metal physical vapor deposition (IMPVD). In this system, an auxiliary plasma source is used in conjunction with a sputter deposition source. The goal is to ionize a significant fraction of the sputtered metal atoms prior to their depositing on the substrate. By applying a bias to the substrate to accelerate metal ions, an anisotropic deposition flux can be produced. The substrate bias serves the additional purpose of providing a sputter flux (either metal ions or buffer gas ions) which competes with deposition, particularly on the lip of the via, and serves to remove encroaching metal atom deposits which could form voids. The IMPVD technique has been developed and demonstrated by Yamashita,¹ and Rossnagel and Hopwood²⁻⁴ for deposition of aluminum and copper. In experiments by Rossnagel and Hopwood, the ionized fraction of the aluminum metal atom flux to the substrate was as large as 90%. A zero-dimensional model of IMPVD has been developed by Hopwood and Qian, and provides results which compare favorably with measurements.⁵

A schematic of a typical IMPVD system is shown in Fig. 1. The metal source is a dc magnetron. The bias applied to

the substrate can be either dc or radio frequency (rf). The secondary ionization source is an rf powered inductive coil immersed in the plasma. In neutral metal PVD, the buffer gas pressure is usually only a few mTorr with the intent of having metal atoms traverse the reactor from target to substrate having few, if any, collisions. In IMPVD, the buffer gas pressure is somewhat higher (many mTorr to 10s mTorr) with the intent of slowing the sputtered metal atoms in the buffer gas and providing the opportunity for them to be ionized. Unfortunately, this also increases the diffusion losses of metal atoms to surfaces other than the substrate. Experimental scaling studies have shown that, for a constant sputtering rate, the fraction of the metal atoms which are ionized increases with increasing buffer gas pressure while the deposition rate decreases.⁵

In this article, we describe and present results from a two-dimensional model for a copper IMPVD system. We show that the deposition rate of metal on the substrate will be reduced as pressure increases due to the increase in diffusive losses. We also show that the sputtering of the auxiliary coils can be a significant issue in IMPVD systems, which must be addressed in a realistic tool design. The model is described in Sec. II, followed by a discussion of our results for a magnetron sputter source with rf inductive coils in Sec. III. Our concluding remarks are in Sec. IV.

II. DESCRIPTION OF THE MODEL

The modeling platform we used in this study was developed at the University of Illinois and is called the hybrid plasma equipment model (HPEM). The HPEM has been previously described in detail,⁶⁻⁹ and so only a brief overview and description of modifications made specifically for this

^{a)}Present address: Materials Research Corp., 2120 W. Guadalupe Rd., Gilbert, AZ 85233-2805;

electronic mail: Michael_Grapperhaus@notes.mrc.sony.com

^{b)}Electronic mail: zoran@grape.amd.com

^{c)}Author to whom correspondence should be addressed; electronic mail: mjk@uiuc.edu

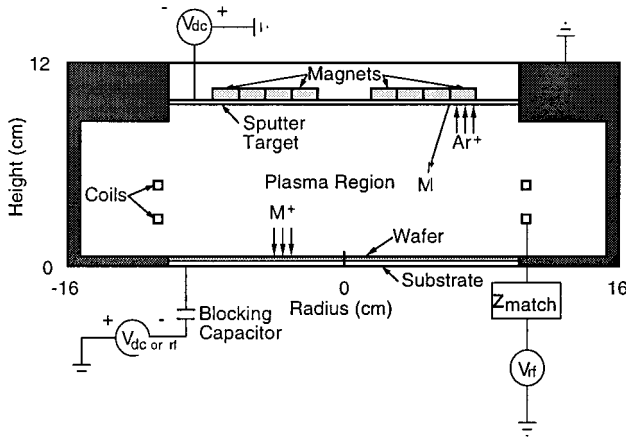


FIG. 1. Schematic of reactor modeled in this study. M denotes metal atoms. The magnetron consists of nested loops of magnetic cusps.

system will be given here. The base two-dimensional (cylindrically symmetric) HPEM consists of an electromagnetic module (EMM), an electron Monte Carlo simulation (EMCS), and a fluid kinetics simulation (FKS). Inductively coupled electric and magnetic fields are computed in the EMM. Those fields are used in the EMCS to generate electron energy distributions as a function of position and phase. The electron distribution is used to generate source rates for electron impact processes and the electron transport coefficients. These parameters are then used in the FKS where momentum and continuity equations are solved for all heavy particles (neutrals and ions). A drift diffusion formulation is used for electrons to enable an implicit solution of Poisson's equation for the electric potential. A one-dimensional semi-analytic sheath model is employed at the plasma-surface boundary to resolve sheaths which have a thickness less than the width of a computational cell in the mesh.⁷ A circuit model is employed to provide biases (dc and rf) on powered surfaces. The species densities and electrostatic fields produced by the FKS are transferred to the EMCS and the EMM. This procedure is iterated to a converged solution.

To address the unique conditions of IMPVD systems, improvements to the HPEM have been made for neutral particle, electron transport, and for defining static magnetic fields. The improvement in neutral particle transport is the addition of a neutral atom slowing down Monte Carlo simulation (NMCS) to account for the long mean free path transport of hot atoms sputtered from the magnetron target. The improvement in electron transport included resolving electron trajectories in regions of high magnetic fields and adding secondary electron emission.

In high magnetic field regions near the magnetron source ($B > 1-3$ kG), the cyclotron frequency is large ($> 3-10$ GHz). Resolving the orbits of electrons around the magnetic fields lines in the EMCS using a simple time stepping routine requires that the time step be a small fraction of the cyclotron period. Doing so leads to unacceptably large computing time. The gyrokinetic approximation, where only the guiding center motion of the electron is followed for conditions where the Larmor radius is small compared to

other dimensions, unfortunately cannot be employed here. The gradient in the magnetic field is large (10s kG/cm) and electrons transition between being highly magnetized near the sputter source to being weakly magnetized near the substrate. There is a corresponding increase in their Larmor radius which violates the gyrokinetic approximation. To avoid using a restrictively small time step in the EMCS, the time stepping technique has been modified. Following the method described in Birdsall and Langdon,¹⁰ the Lorentz equation is rearranged by defining intermediate velocities, v^- and v^+ :

$$v_{t-\Delta t/2} = v^- - \frac{q\mathbf{E}_\perp}{m} \frac{\Delta t}{2} \quad (1)$$

$$v_{t+\Delta t/2} = v^+ + \frac{q\mathbf{E}_\perp}{m} \frac{\Delta t}{2}, \quad (2)$$

where \mathbf{E}_\perp is the component of the electric field perpendicular to the magnetic field. v^- and v^+ are the velocities before and after the magnetic field rotation. Putting these expressions into the finite difference Lorentz equation yields

$$\frac{v^+ - v^-}{\Delta t} = \frac{q}{2m} (v^+ + v^-) \times \mathbf{B} \quad (3)$$

which can be solved using geometric considerations. This gives an explicit solution method for updating the implicit Lorentz equation. This modification increases the allowable time step in the EMCS by a factor of approximately 20 over a direct finite time differencing.

When using biases for either the target or substrate, secondary emission of electrons is an important and necessary source of electrons. The secondary emission of electrons from all surfaces was therefore included in the EMCS. The procedure we followed is to launch electrons from the surface of an electrode (or other specified surface) at a rate determined by the local ion current to the surface and a secondary electron emission coefficient. When using the semi-analytic sheath model, in which the sheath is thin compared to electron mean free paths, electrons are assumed to traverse the sheath collisionlessly. The electron pseudoparticles are therefore launched perpendicular to the surface with an energy equal to the local sheath potential. When not using the sheath model, electrons are launched with a small energy (typically 4 eV) and a Lambertian angular distribution. The trajectories of the secondary electrons and their progeny are tracked using the same algorithms as in the EMCS for bulk electrons (or an injected electron beam)¹¹ until they slow below a specified energy, typically 3.6 eV (90% of initial energy), thereby joining the bulk electrons. The spatially dependent rate of electrons slowing into the bulk is then included as a source term for electrons in the FKS. The electron energy distribution for the secondary electrons is separately computed and used to generate source functions for electron impact excitation and ionization. These source functions are then used in the FKS.

Metal atoms sputtered from the magnetron target have an initial energy of a few eV and have a mean free path as long as a few cm. These characteristics make a fluid description for their transport questionable. In addition, the disparate energy distribution of the sputtered atoms compared to

the bulk metal atoms requires that the influx of metal atoms be represented as a separate group. Therefore, a kinetic Monte Carlo approach, the NMCS, was used to track sputtered metal atoms from the surface until they either slow down to thermal speeds or strike a surface (assuming a unity sticking coefficient). This allows the kinetic effects of the neutrals to be represented during the initial slowing of the sputtered neutrals, while allowing the use of the more efficient fluid equations for the thermal diffusion process.

Sputtered atoms are assumed to be emitted from the surface of the target with a cosine angular distribution. Since we are not resolving the sputter erosion track, the magnetron surface is assumed to be planar. The emitted atoms are given an energy specified by Thompson's law¹² which, for incident ions of several hundred eV, can be approximated with a simple cascade distribution,

$$p(E) = \frac{2E_b}{E^2(1+E_b/E)^3}, \quad (4)$$

where $p(E)$ is the relative probability of emitting an atom of energy E and E_b is the surface binding energy, which typically ranges from 1 to 4 eV.¹³

In the NMCS, Monte Carlo particles are launched from each point along the magnetron target surface with energies and directions selected from these distributions. The trajectories of the atoms are then tracked as they move through the plasma region and undergo collisions with the plasma species. Only momentum transfer collisions with the background gas atoms are considered. Collisions are modeled as hard sphere collisions in the center of mass reference frame. The collision cross section is computed based on the Lennard–Jones radius of the atoms. For energetic neutrals, this results in forward peaked scattering. The trajectories are followed until they slow to thermal speeds, or until they strike a surface. The ending location of the particles is tallied to generate a Green's function $G(r, r')$ designating the spatial distribution of atoms slowing to thermal speeds at a location r within the plasma volume originating from location r' on the target.

The sputtering rate at each location along the target is determined by the local ion flux to the surface. In addition, charge exchange reactions near the target surface produce fast neutrals, which can also sputter target atoms. To account for sputtering by fast neutrals, all charge exchange reactions of ions directed towards the surface which occurs in the mesh cell adjacent to the target are assumed to generate hot neutrals which contribute to sputtering. This approximation was made based on the fact that these ions have already traversed a large fraction of the presheath. Therefore, the fast neutral flux produced by charge exchange is computed by multiplying the incident ion flux times the neutral atom density, the charge exchange cross section, and the width of the last cell. The total sputter rate is, then, the ion flux to the surface plus the fast neutral flux times the sputter yield. The sputter yield is assumed to be constant across the target for a given incident ion and material composition. The sputter rate which so computed is then convolved with the Green's function for slowing down generated in the NMCS to determine the spatially dependent source rates of sputtered atoms

entering the fluid. One can show that in virtually all plasmas of interest (pressures of 10–40 mTorr, electron densities 10^{11} – 10^{12} cm⁻³), the probability that a sputtered atom undergoes excitation or ionization prior to thermalizing is small, and so these processes are ignored in the NMCS.

Capabilities were also added to compute the static magnetic fields as employed in the magnetron sputter source. Magnetrons are typically constructed from lines of permanent magnets. These magnets were represented by “filling” a specified material in the numerical mesh with arrays of small current loops (current density \mathbf{j}) oriented in the appropriate direction to provide the desired orientation of the magnetic field. The current loops then provided source terms in solving for vector potential, \mathbf{A} , which, by differentiation, yielded the static magnetic fields,

$$\nabla \times \frac{1}{\mu} \nabla \times \mathbf{A} = \mathbf{j}, \quad \mathbf{B} = \nabla \times \mathbf{A}, \quad (5)$$

where μ is the local permeability. We solved for the vector potential as a boundary value problem using the method of successive over relaxation by extending the numerical mesh to dimensions twice that shown in Fig. 1, and setting $A = 0$ on the boundaries.

When using drift-diffusion formulations in the FKS, diffusivities and mobilities for all charged species were then resolved into components parallel and perpendicular to the local magnetic field. This was accomplished by defining radial and axial mobilities where, for example,

$$\mu_r = \mu_0 \frac{1 + (qB_r/mv_m)^2}{1 + (qB/mv_m)^2}, \quad (6)$$

where μ_r is the mobility for radial transport, μ_0 is the isotropic mobility, B_r is the radial component of the magnetic field, B is total magnitude of the field, and v_m is the momentum transfer collision frequency.

Electron impact cross sections and ion mobilities for the metal systems of interest are not well characterized. For example, few electron impact cross sections are available for Al and Ti, which are of particular interest in the semiconductor industry. The knowledge base for Cu is fairly well characterized because of past interest in copper vapor lasers.^{14,15} The lack of a complete cross section set and gas phase rate coefficients for Al and Ti presents difficulty in modeling, and therefore we have modeled a Cu IMPVD system with the intention of characterizing the general behavior of IMPVD systems.

The complexity of the atomic structure of the Cu atom requires some simplifications in order to reduce the magnitude of computations needed. Therefore, within the FKS, the excited states of copper are lumped into an effective excited state denoted as Cu*, which has the characteristics of Cu[²D_{5/2}]. The higher excited states were not explicitly tracked within the FKS because of their relatively short radiative decay time¹⁴ and their low rate of excitation compared to the Cu[²D_{5/2}] level. This was done to eliminate the necessity of tracking several excited states of Cu, while maintaining the important processes. Several runs were performed with and without the higher excited states in the FKS and the results were essentially the same. Within the EMCS,

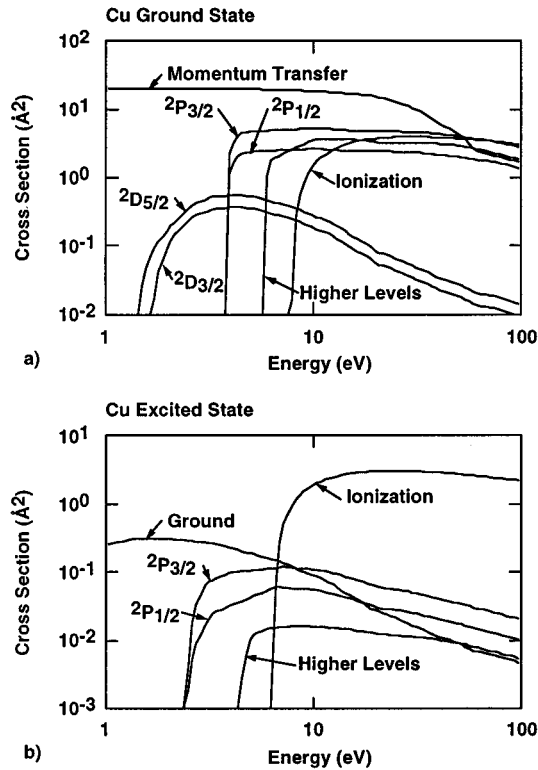


FIG. 2. Cu electron impact cross sections. (a) Excitations from the ground state. (b) Excitations from $\text{Cu}[^2D_{5/2}]$, our effective Cu^* .

however, electron impact excitations from the ground state ($^2S_{1/2}$), to the metastable states ($^2D_{5/2}$, $^2D_{3/2}$), resonance states ($^2P_{1/2}$ and $^2P_{3/2}$), and a pseudostate representing higher levels; and from the metastable $\text{Cu}^*[^2D_{5/2}]$ to the resonance states ($^2P_{1/2}$ and $^2P_{5/2}$) and pseudostate, are included for the purposes of determining the electron energy distribution functions. Cross sections are essentially the same as those used in Ref. 15, except that the ionization cross section from the ground state was from curve fits by Carman,¹⁶ based on published data of Sheibner, Hazi, and Henry¹⁷ and on unpublished raw data of Sheibner and Hazi.¹⁸ The electron impact cross sections we used are shown in Fig. 2. Heavy body reaction rates were obtained from Ref. 15 and a summary of the Ar/Cu reactions used is shown in Table I.

III. PLASMA BEHAVIOR IN AN IONIZED METAL SPUTTER DEPOSITION REACTOR

The geometry we used in our simulations is shown in Fig. 1 and is based on the experiments of Yamashita¹ and of Rosnagel and Hopwood.^{2,3} It consists of a 20-cm-diam dc magnetron sputter source with an applied voltage of -250 V on the target. Due to the limitations of our two-dimensional simulation, only a circular magnet configuration can be modeled. The circular sputter track is defined using cusp magnet rings above the sputter target. The chamber height is 9 cm. A two turn solenoid, powered at 13.56 MHz, is immersed in the plasma and deposits 1 kW of inductively coupled power. (In all instances, the term “power deposition” refers to the net

TABLE I. Ar/Cu chemistry.

Reaction ^a	Rate coefficient ($\text{cm}^3 \text{s}^{-1}$)	Reference
$e + \text{Ar} \rightarrow \text{Ar} + e$	b	19
$e + \text{Ar} \rightarrow \text{Ar}[4s] + e$	b	20
$e + \text{Ar} \rightarrow \text{Ar}[4p] + e$	b	20
$e + \text{Ar} \rightarrow \text{Ar}^+ + e + e$	b	21
$e + \text{Ar}[4s] \rightarrow \text{Ar}^+ + e + e$	b	22
$e + \text{Ar}^+ \rightarrow \text{Ar}^+ + e$	b	23
$e + \text{Cu} \rightarrow \text{Cu} + e$	b	15
$e + \text{Cu} \rightarrow \text{Cu}[^2D_{5/2}] + e$	b	15
$e + \text{Cu} \rightarrow \text{Cu}[^2D_{3/2}] + e$	b	15
$e + \text{Cu} \rightarrow \text{Cu}[^2P_{1/2}] + e$	b	15
$e + \text{Cu} \rightarrow \text{Cu}[^2P_{3/2}] + e$	b	15
$e + \text{Cu} \rightarrow \text{Cu}[\text{pseudostate}] + e$	b	15
$e + \text{Cu} \rightarrow \text{Cu}^+ + e + e$	b	16
$e + \text{Cu}[^2D_{5/2}] \rightarrow \text{Cu}[^2D_{5/2}] + e$	b	15
$e + \text{Cu}[^2D_{5/2}] \rightarrow \text{Cu}[^2P_{1/2}] + e$	b	15
$e + \text{Cu}[^2D_{5/2}] \rightarrow \text{Cu}[^2P_{3/2}] + e$	b	15
$e + \text{Cu}[^2D_{5/2}] \rightarrow \text{Cu}[\text{pseudostate}] + e$	b	15
$e + \text{Cu}[^2D_{5/2}] \rightarrow \text{Cu}^+ + e + e$	b	15
$\text{Ar}^* + \text{Ar}^* \rightarrow \text{Ar}^+ + \text{Ar} + e$	5×10^{-10}	24
$\text{Cu}^* + \text{Cu} \rightarrow \text{Cu} + \text{Cu}$	1×10^{-12}	c
$\text{Cu}^* + \text{Cu}^* \rightarrow \text{Cu}^* + \text{Cu}$	1×10^{-12}	c
$\text{Ar}^* + \text{Cu} \rightarrow \text{Ar} + \text{Cu}^+ + e$	5×10^{-11}	c
$\text{Ar}^* + \text{Cu}^* \rightarrow \text{Ar} + \text{Cu}^+ + e$	5×10^{-11}	c
$\text{Ar}^+ + \text{Cu} \rightarrow \text{Ar} + \text{Cu}^+ + e$	5×10^{-10}	c
$\text{Ar}^+ + \text{Cu}^* \rightarrow \text{Ar} + \text{Cu}^+ + e$	5×10^{-10}	c
$\text{Cu}^+ + \text{Cu} \rightarrow \text{Cu} + \text{Cu}^+$	6×10^{-10}	c
$\text{Ar}^+ + \text{Ar} \rightarrow \text{Ar} + \text{Ar}^+$	1×10^{-9}	c

^aIn the FKS, all excitations of Ar are lumped into Ar^* , which is effective $\text{Ar}[4s]$, and all excitations of Cu are lumped into Cu^* , which is effectively $\text{Cu}[^2D_{5/2}]$.

^bRate coefficients are calculated from electron energy distribution obtained in the EMCS.

^cEstimated.

power deposited in the plasma through charged particle acceleration.) The intended purpose of the solenoid power is to ionize the sputtered metal atoms. The substrate is biased at -20 V dc to accelerate ions toward the surface. Due to the biasing of the coils (described below), ions can obtain sufficient energy to sputter the coils, which we assume to be made of copper. Therefore, sputtering of copper atoms occurs from both the target and the coils. (Sputtering from the coils is computationally treated in the same manner as sputtering from the target. A Green’s function is produced by the NMCS for starting locations of sputtered atoms from the surface of the coil. When combined with the computed ion flux to the coils, we obtain the volumetric source of sputtered copper atoms.) The Ar fill pressure is varied from 15 to 45 mTorr. The sputter parameters we used were $E_b = 3.5$ eV and a sputter yield = 2.0.

Since the coils are immersed directly in the plasma, they function equivalently to electrodes in a reactive ion etching (RIE) system with respect to biasing of the plasma potential and heating the plasma, and so their electrical coupling to the plasma must be considered. As a result, we resolve the rf cycle in the FKS. The details of this coupling depend on the configuration of the driving circuitry of the coils, a topic which is beyond the scope of the present study. We have

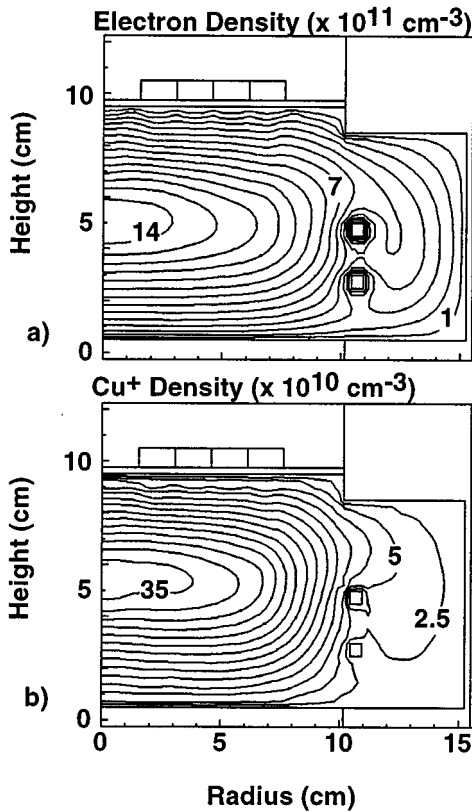


FIG. 3. Electron and Cu^+ ion density for an IMPVD at 35 mTorr, with -250 V on the sputter target, 1 kW inductive power, and -20 V applied to the substrate. (a) Electron density. Contours values are $\times 10^{11} \text{ cm}^{-3}$. (b) Cu^+ ion density. Contours values are $\times 10^{10} \text{ cm}^{-3}$. The Cu^+ density is $\approx 25\%$ of the total ion density.

therefore simply specified the amplitude of the rf potential the coils to be 100 V , (200 V peak-to-peak), which we acknowledge to be a lower limit, and that there be a single blocking capacitor in series with power supply upon which a dc bias is collected. Since the area ratio (coil to wall) is very large, the dc bias typically is nearly the rf amplitude.

The electron density and Cu^+ density are shown in Fig. 3, for 35 mTorr Ar fill pressure. The electron density has a peak value of $1.4 \times 10^{12} \text{ cm}^{-3}$, which is somewhat higher than that obtained in a similar size and powered inductively coupled etching reactors, and is likely due to the low ionization potential of Cu (7.49 eV). Although the primary ionization source for the electrons is near the coils where the inductive power deposition peaks, the large aspect ratio and lack of volumetric sources of electron loss (such as attachment or dissociative recombination) leads to the electron density peaking on axis. (In all instances, the term “source” refers to the volume production of particular species expressed as particles/ $\text{cm}^3 \text{ s}$.) The source of ions due to electron impact ionization near the coils is $6 \times 10^{16} \text{ cm}^{-3} \text{ s}^{-1}$ for a power deposition of 1300 W from capacitive and inductive coupling of the coils. The ionization source near the magnetron is $5 \times 10^{15} \text{ cm}^{-3} \text{ s}^{-1}$ for an applied magnetron power deposition of 1700 W . The ionization source near the magnetron is smaller inspite of the higher magnetron power

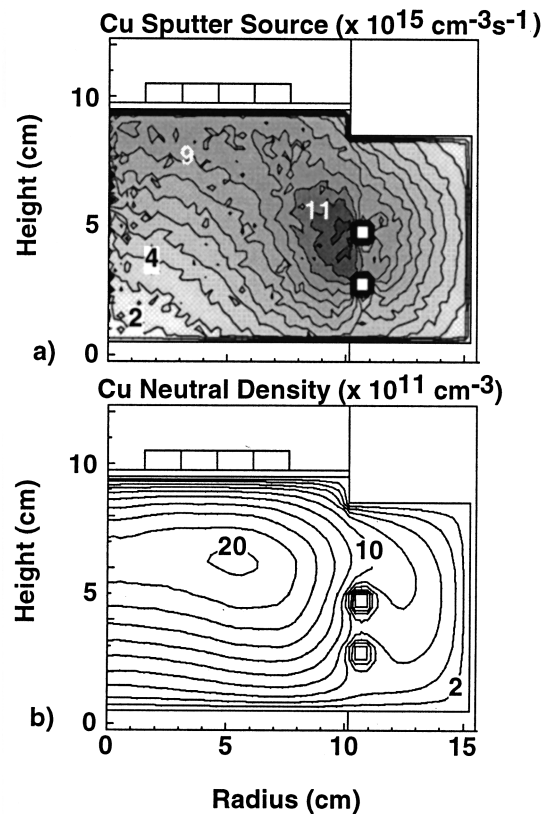


FIG. 4. Neutral copper properties. (a) Source of sputtered atoms which have slowed to thermal speed. Contours values are $\times 10^{15} \text{ cm}^{-3} \text{ s}^{-1}$. (b) Cu neutral density, including both ground state and excited state atoms. Contours values are $\times 10^{11} \text{ cm}^{-3}$. The Cu density peaks off axis due to coil sputtering.

deposition because the majority of the power goes into ion acceleration across the sheath rather than electron excitation. Contributions to the ionization source from secondary emission are displaced into the bulk. The magnetron functions as an externally sustained discharge where ionization, and hence current to the target, is largely determined by the inductive coil heating. At the operating pressure of 35 mTorr, the electron collisionality is much higher than at a few mTorr where traditional sputter magnetrons operate. This collisionality somewhat compromises the trapping of electrons in the closed track of the magnetron and produces a diffusive charged density profile, rather than a well confined source beneath the sputter target. Some scalloping of the electron density in the cusps of the magnetron can be seen. The Cu^+ density has a peak value of $3.5 \times 10^{11} \text{ cm}^{-3}$, approximately 25% of the total ion density, and has a profile centered on axis, following the electron density.

The source of sputtered Cu atoms and the total Cu neutral atom density are shown in Fig. 4. The Cu atom sputter source is the rate at which atoms sputtered from the surface slow down into the thermal group, making the transition from kinetic transport to fluid transport. The sputter source is peaked near the radial edge of the plasma zone, a consequence of the high rate of sputtering from the coils. The peak value of the source of sputtered Cu atoms is $1.5 \times 10^{16} \text{ cm}^{-3} \text{ s}^{-1}$. This high rate of sputtering from the coils is sustained by the large amount of power deposition near the

vicinity of the rf coils. This produces a high ion flux back onto the surface of the coils which, combined with the large sheath potential, produces sputtering. The total Cu neutral density, which includes ground state and excited state Cu atoms, is shown in Fig. 4(b). The peak value for the neutral Cu is $2.0 \times 10^{12} \text{ cm}^{-3}$ and is peaked off axis below the magnets. The off axis peak is caused by the high sputtering rate from the coils as well as by the off axis sputtering source from the target. Due to the fact that the lowest excited states of Cu are metastable yet have a large excitation rate due to their low threshold energy (1.4 eV), a large fraction of the Cu atoms are excited, in this case approximately 25%.

The importance of sputtering of the coil as a source of metal atoms has recently been confirmed in experiments by Wang *et al.*²⁵ In these experiments, a Cu dc magnetron source was used in an IMPVD reactor having aluminum coils. Optical emission from excited Cu and Al states indicated comparable densities of each metal. Surface analysis of the resulting film showed that, depending on conditions, comparable fractions of aluminum and copper were obtained. It has also been reported that the uniformity of metal atom deposition is a function of inductive power deposition, an effect attributed to coil sputtering.²⁶

The fluxes of Cu species to the wafer surface for 35 mTorr Ar fill pressure are shown in Fig. 5(a) while including sputtering from the coil and assuming that all Cu species have a unity sticking coefficient. The unthermalized flux is the flux of sputtered atoms which have traversed the reactor from the target to the substrate without undergoing sufficient collisions to slow to thermal speeds. The unthermalized flux is strongly peaked at the outer edge of the wafer because of the high rate of sputtering from the nearby coils and the off axis circular sputter track on the target. The thermalized Cu neutral flux has much less variation although it is slightly peaked at ≈ 7.5 cm from the axis. The more uniform thermal Cu flux compared to the unthermalized flux is due to the diffusivity of Cu atoms in the plasma. The ion flux is relatively uniform at small radii, but tapers off at larger radius. From experience with designing conventional ICP plasma sources, one can recoup some of this uniformity by a combination of operating with a somewhat squatter aspect ratio, whose value is a sensitive function of pressure, and by changing the position of the rf coils. The flux of the Cu^* is relatively uniform across the wafer and approximately 13% of the total. The total deposition flux of Cu is the sum of the fluxes of all neutral (thermal and hot) and ionized Cu species. The total flux increases at larger radius because of the unthermalized neutral component, although the flux of the other components are decreasing.

The fraction of the Cu flux to the wafer which is ionized is $\approx 50\%$ near the center of the wafer. It decreases at larger radii due to the increase in the unthermalized component of the neutral flux produced by the proximity of the coils. To prevent this trend, one must either minimize sputtering from the coil, place the coils sufficiently far from the wafer that the sputtered atom flux has opportunity to thermalize and be ionized prior to striking the substrate, or place the coils outside the chamber. The coils can be placed outside the chamber by using an appropriately designed Faraday shield which

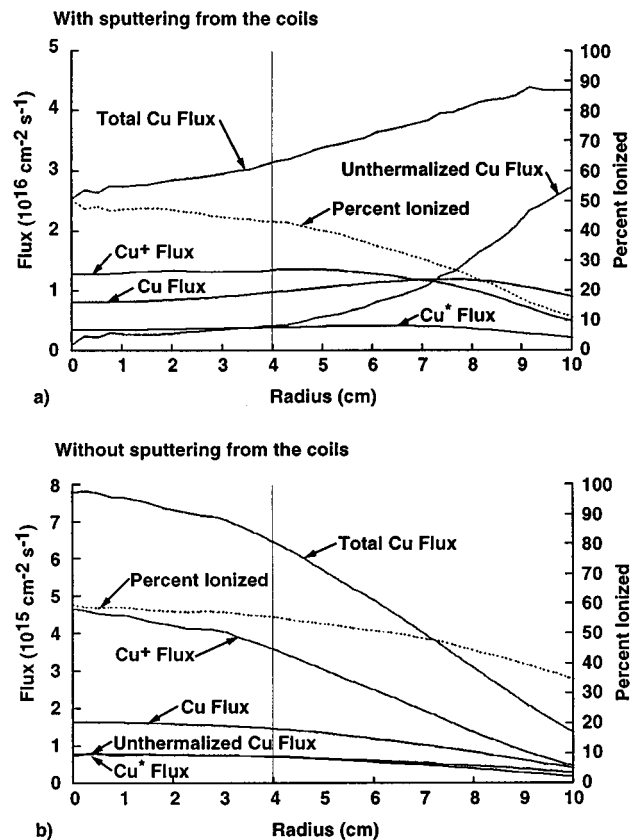


FIG. 5. Cu deposition flux to the substrate and fraction of the flux which is ionized. The neutral flux consists of contributions from Cu ground state, Cu^* , and the unthermalized sputter flux. (a) Fluxes with sputtering from the coils. (b) Fluxes without sputtering from the coils. Coil sputtering produces an off axis maximum in the Cu atom flux.

is not electrically shorted by depositing metal atoms.²⁷

The same conditions were simulated with the exception that we specified that there be no sputtering from the coils. The electron density and Cu^+ densities for this case are shown in Fig. 6. The Cu^+ density has a peak value of $1.1 \times 10^{11} \text{ cm}^{-3}$, which is significantly smaller and more strongly peaked on axis than in the case with coil sputtering. This trend is due to a decrease in neutral copper density, especially near the coils. The electron density has a peak value of $1.2 \times 10^{12} \text{ cm}^{-3}$, slightly smaller than that when including coil sputtering, however it is more spatially uniform due to a more uniform ionization rate. Although Cu is more easily ionized than Ar, it also has a larger rate of momentum transfer and a larger rate of inelastic energy loss. Therefore, an increase in copper density, in this case caused by including sputtering from the coils, results in more cooling of electrons by collisions with copper atoms. This results in the electron temperature being more peaked near the heating source at the coils.

The copper sputter source and neutral density are shown in Fig. 7 for the case where no sputtering is allowed from the coils. The sputter source has a peak value of $5.5 \times 10^{15} \text{ cm}^{-3} \text{ s}^{-1}$ which is smaller than the case where sputtering is allowed from the coils. (The total sputter rate for a

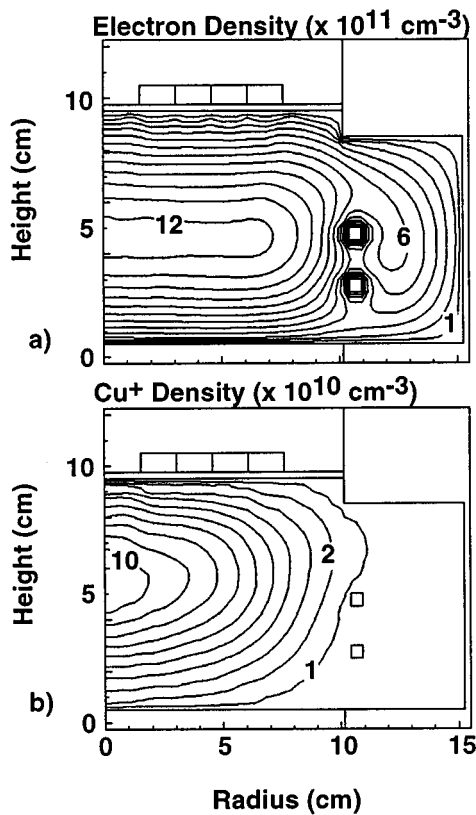


FIG. 6. Electron and Cu^+ ion density without sputtering from the coils. (a) Electron density. Contours values are $\times 10^{11} \text{ cm}^{-3}$. (b) Cu^+ ion density. Contours values are $\times 10^{10} \text{ cm}^{-3}$.

fixed sputter yield, which has been assumed in this model, depends only on the total flux of ions to the surface. In the case where sputtering from the coils is allowed, the contributions from the coils actually exceeds the contributions from the target.) The peak in the sputter source is located below the magnetron target, although it is not located directly beneath the magnets. This condition results from the relatively uniform sputter source from the target, combined with the short mean free path of the neutrals in a cylindrical geometry, leading to a source peaked on axis. Since our simulation is only two-dimensional, the magnetron tracks are at best nested circular loops. Sputtering is therefore directly proportional to the ion flux incident onto the target. In many commercial magnetrons, the “racetrack” cuts across radii, thereby “mixing” incident ion fluxes from different radii. The total neutral Cu density in the plasma has a peak value of $4.6 \times 10^{11} \text{ cm}^{-3}$. The Cu density for this case is significantly lower and more sharply peaked on axis than when sputtering from the coils is allowed, thereby emphasizing the importance of considering this source of metal atoms in reactor design.

The deposition fluxes as a function of radius are shown in Fig. 5(b) when no sputtering is allowed from the coils. As expected, all incident fluxes fall off at larger radius, since there is no secondary source of sputtered Cu from the coils. The overall deposition flux without sputtering from the coils is significantly lower than when sputtering from the coils is

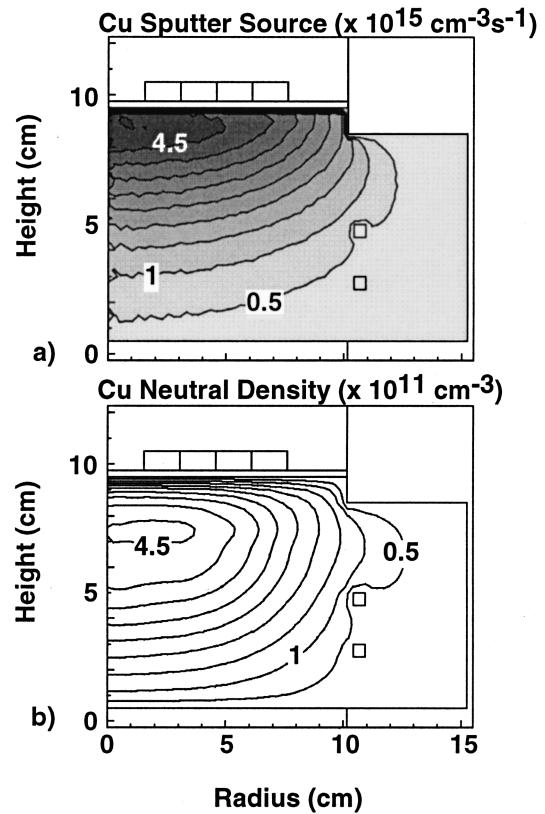


FIG. 7. Cu sputter source and density without sputtering from the coils. (a) Source of sputtered atoms which have slowed to thermal speeds. Contours values are $\times 10^{15} \text{ cm}^{-3} \text{ s}^{-1}$. (b) Cu neutral density, including both ground state and excited state atoms. Contours values are $\times 10^{11} \text{ cm}^{-3}$. The absence of copper sputtering from the coils results in an on axis maximum in Cu density.

allowed, which in turn leads to a slightly higher percent of the flux which is ionized, $\approx 60\%$ on axis. This results from there being less cooling of the electrons in the plasma when the Cu density is low. The unthermalized flux in this case is only a small fraction of the total flux to the surface, which indicates that the combination of reactor height and pressure for this case provides for sufficient thermalization of the sputtered atoms in the plasma volume, provided that the sputter target is the primary source of copper in the system.

The variations of the Cu ionized fraction and total deposition flux to the wafer with fill pressure and target voltage are shown in Fig. 8. To offset the influence of sputtering from the coils, values are averaged over the inner 4 cm radius of the wafer, as shown by the vertical line in Fig. 5. As the pressure increases, the mean free path of the atoms decreases. The fraction of sputtered atoms which slow down into the plasma increases, allowing more of them to be ionized before reaching the wafer. The ionized fraction of the flux to the wafer increases from $\approx 29\%$ at 15 mTorr to $\approx 47\%$ at 45 mTorr. At the same time, increasing pressure has the effect of dispersing the atoms due to diffusion, which results in a lower deposition rate, since more of the sputtered atoms are lost to other surfaces in the reactor. The deposition flux decreases from $\approx 5.5 \times 10^{16} \text{ cm}^{-2} \text{ s}^{-1}$ ($3900 \text{ \AA}/\text{min}$) at 15 mTorr to $\approx 1.5 \times 10^{16} \text{ cm}^{-2} \text{ s}^{-1}$ ($1100 \text{ \AA}/\text{min}$) at 45 mTorr. This implies a trade off between ionized flux fraction and deposition rate, which for this geometry and operating

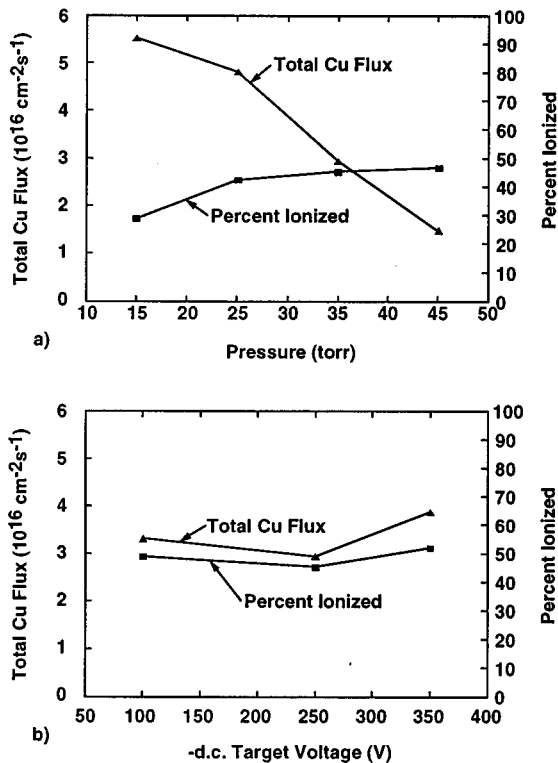


FIG. 8. Cu deposition flux and fraction of the flux which is ionized (a) as a function of pressure and (b) as a function of dc voltage on the target. Increasing pressure reduces the Cu flux but increases the fraction ionized.

conditions would be between 25 and 35 mTorr. This result agrees qualitatively with the ionized Al experiments of Rossnagel and Hopwood.^{2,3} Experiments by Yamashita with a 5 cm gap between the target and the substrate, at 10 mTorr and 800 W dc target power produced a deposition rate of 11 200 Å/min for Cu deposition.¹

The variations of Cu deposition flux and the ionized flux fraction with target voltage is shown in Fig. 8(b). In these cases, the sputter yield was assumed to remain constant, so that the main effect of increasing the target voltage is to increase the rate of plasma generation near the magnetron surface due to secondary electron emission. The deposition flux does not change appreciably between the -100 and the -250 V cases, which implies that at this operating point the ion flux to the target is roughly the same between the two cases. As the voltage is increased to -350 V, the deposition rate experiences a small increase due to a slightly larger rate of ionization by secondary electrons leading to larger rates of Cu sputtering, although the ionized flux fraction remains near 50%.

By moving the coils further away from the substrate, it is expected that uniformity of the Cu flux will improve by reducing the unthermalized Cu flux resulting from coil sputtering. This is shown in Fig. 9, Cu fluxes are plotted when the coils have been raised 1.5 cm towards the target compared to the standard case. The Cu^+ flux is nearly the same as seen in the standard case [Fig. 5(a)]. The main difference between this case and the standard case is that the neutral fluxes are smaller. The unthermalized flux is substantially reduced, es-

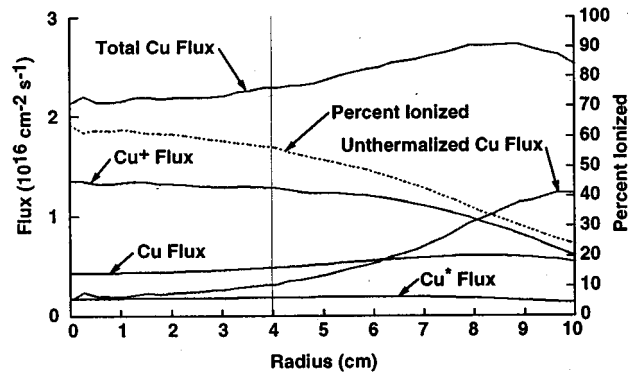


FIG. 9. Deposition fluxes and fraction of the flux which is ionized when the coils are raised 1.5 cm toward the sputter target.

pecially at the outer radius, with a peak value of $\approx 1.2 \times 10^{16} \text{ cm}^{-2} \text{ s}^{-1}$ (850 Å/min) at the outer radius compared to $\approx 2.8 \times 10^{16} \text{ cm}^{-2} \text{ s}^{-1}$ (2000 Å/min) in the standard case. The other neutral fluxes are also smaller resulting in a total deposition flux which is smaller, and somewhat more uniform. Since the coils have been moved closer to the top of the reactor, diffusion losses of sputtered Cu atoms are larger. As the ionized flux is nearly the same, these conditions lead to a higher ionized percentage, $\approx 62\%$ on the axis.

IV. CONCLUDING REMARKS

A two-dimensional model for ionized metal physical vapor deposition has been developed, and has been applied to the investigation and design of deposition devices for Cu deposition. For a modified magnetron sputter source, pressure plays an important part in determining the transport of sputtered atoms. At low pressure, the sputtered atoms traverse the reactor with few collisions before reaching the wafer, while at higher pressure, the transport becomes diffusive, which allows for ionization for the metal atoms. However, the increase in pressure creates a diffusive loss mechanism for atoms to the walls, which reduces the deposition rate. Sputtering from the coils is seen to be a significant source of metal atoms. Sputtering from the coils is produced by the high plasma density generated near the coils from inductive heating followed by ion acceleration into the coils. This source of metal atoms must also be considered when optimizing the uniformity of the deposition flux to the substrate. Sputtering from the coils may limit the lifetime of the coils, however the total erosion rate will ultimately be determined by the difference between deposition onto the coils and sputtering. These results emphasize the need for careful choice of coil location, coil material, and circuit parameters to optimize operation.

ACKNOWLEDGMENTS

The authors would like to thank R. J. Carman, K. F. Sheibner, and A. U. Hazi for their help with the Cu ionization cross section. This work supported by the Semiconductor Research Corporation, National Science Foundation (Grant No. ECS 94-04133, CTS 94-12565), Office of Naval Research (Grant No. N00014-94-1-0819), and the University of Wisconsin Engineering Research Center for Plasma Aided Manufacturing.

- ¹M. Yamashita, *J. Vac. Sci. Technol. A* **7**, 151 (1989).
- ²S. M. Rossnagel and J. Hopwood, *Appl. Phys. Lett.* **63**, 3285 (1993).
- ³S. M. Rossnagel and J. Hopwood, *J. Vac. Sci. Technol. B* **12**, 449 (1994).
- ⁴S. M. Gorbalkin, D. B. Poker, R. L. Rhoades, C. Doughty, L. A. Berry, and S. M. Rossnagel, *J. Vac. Sci. Technol. B* **14**, 1853 (1996).
- ⁵J. Hopwood and F. Qian, *J. Appl. Phys.* **78**, 758 (1995).
- ⁶S. Rauf and M. J. Kushner, *J. Appl. Phys.* **81**, 5966 (1997).
- ⁷M. Grapperhaus and M. J. Kushner, *J. Appl. Phys.* **81**, 569 (1997).
- ⁸W. Z. Collison and M. J. Kushner, *Appl. Phys. Lett.* **68**, 903 (1996).
- ⁹P. L. G. Ventzek, M. Grapperhaus, and M. J. Kushner, *J. Vac. Sci. Technol. B* **12**, 3118 (1994).
- ¹⁰C. K. Birdsall and A. B. Langdon, *Plasma Physics Via Computer Simulation* (McGraw-Hill, New York, 1985).
- ¹¹M. J. Kushner, W. Z. Collison, and D. N. Ruzic, *J. Vac. Sci. Technol. A* **14**, 2094 (1996).
- ¹²T. Heberlein, G. Krautheim, and W. Wuttke, *Vacuum* **42**, 47 (1991).
- ¹³M. A. Lieberman and A. J. Lichtenberg, *Principles of Plasma Discharges and Materials Processing* (Wiley, New York, 1994).
- ¹⁴R. J. Carman, D. J. W. Brown, and J. A. Piper, *IEEE J. Quantum Electron.* **30**, 1876 (1994).
- ¹⁵M. J. Kushner and B. E. Warner, *J. Appl. Phys.* **54**, 2970 (1983).
- ¹⁶R. J. Carman (private communication).
- ¹⁷K. F. Sheibner, A. U. Hazi, and R. J. W. Henry, *Phys. Rev. A* **35**, 4869 (1987).
- ¹⁸K. F. Sheibner and A. U. Hazi (private communication).
- ¹⁹M. Hayashi, Nagoya Institute of Technology Report No. IPPJ-AM-19 (1991).
- ²⁰K. Tachibana, *Phys. Rev. A* **34**, 1007 (1987).
- ²¹D. Rapp and P. Englander-Golden, *J. Chem. Phys.* **43**, 1464 (1965).
- ²²R. H. McFarland and J. D. Kinney, *Phys. Rev.* **137**, A1058 (1965).
- ²³M. Mitchner and C. Kruger, *Partially Ionized Gases* (Wiley, New York, 1973), Chap. 2.
- ²⁴P. K. Leichner and R. J. Ericson, *Phys. Rev. A* **9**, 251 (1974).
- ²⁵W. W. Wang, J. E. Foster, M. Grapperhaus, A. E. Wendt, J. Booske, and M. J. Kushner, Division of Plasma Physics Annual Meeting, November 1997 (unpublished).
- ²⁶P. Gopalraja, Y. Tanaka, K. Tanimoto, J. Forster, and Z. Xu, *Ionized Physical Vapor Deposition of Titanium and Titanium Nitride*, Paper K1.7 (Materials Research Society Sprint 1997 Symposium, San Francisco, 1997).
- ²⁷R. Bayer, A. D. Lantsman, and J. A. Seirmarco, US Patent 5,569,363 (October 1996).